Title
Multivariate Machine Learning Models of Nanoscale Porosity from Ultrafast NMR Relaxometry

Journal
Angewandte Chemie International Edition, 63(13)

ISSN
1433-7851

Authors
Fricke, Sophia N
Salgado, Mia
Menezes, Tamires
et al.

Publication Date
2024-03-22

DOI
10.1002/anie.202316664

How to cite: *Angew. Chem. Int. Ed.* **2024**, *63*, e202316664
doi.org/10.1002/anie.202316664

Porosity Hot Paper

Multivariate Machine Learning Models of Nanoscale Porosity from Ultrafast NMR Relaxometry

Sophia N. Fricke, Mia Salgado, Tamires Menezes, Kátilla M. Costa Santos, Neal B. Gallagher, Ah-Young Song, Jieyu Wang, Kaitlyn Engler, Yang Wang, Haiyan Mao, and Jeffrey A. Reimer*

Abstract: Nanoporous materials are of great interest in many applications, such as catalysis, separation, and energy storage. The performance of these materials is closely related to their pore sizes, which are inefficient to determine through the conventional measurement of gas adsorption isotherms. Nuclear magnetic resonance (NMR) relaxometry has emerged as a technique highly sensitive to porosity in such materials. Nonetheless, streamlined methods to estimate pore size from NMR relaxometry remain elusive. Previous attempts have been hindered by inverting a time domain signal to relaxation rate distribution, and dealing with resulting parameters that vary in number, location, and magnitude. Here we invoke well-established machine learning techniques to directly correlate time domain signals to BET surface areas for a set of metal-organic frameworks (MOFs) imbibed with solvent at varied concentrations. We employ this series of MOFs to establish a correlation between NMR signal and surface area via partial least squares (PLS), following screening with principal component analysis, and apply the PLS model to predict surface area of various nanoporous materials. This approach offers a high-throughput, non-destructive way to assess porosity in c.a. one minute. We anticipate this work will contribute to the development of new materials with optimized pore sizes for various applications.

Introduction

The function of many porous materials designed for gas adsorption, separation, or catalysis is closely tied to their pore structure and geometry. Indeed, nanoporous materials are ubiquitous in a wide sector of chemistries, from processing to environmental remediation.[1,2] Despite the importance of their role, though, scientists lack an efficient screening tool to measure the size of nanopores in a high-throughput manner. Gas adsorption isotherms are largely the most common technique; however, they are time-intensive to obtain—often requiring up to a day—and are prone to inaccuracies if a material deviates from the assumed mono-layer surface adsorption model.[3–5] Because porous networks are known to be archetypal fractal objects,[6,7] often with surface complexity greater than 2D,[8–10] an assumption of mono-layer surface adsorption is not universally valid and may lead to systematic error[11,12] in surface area and pore volume predictions.

NMR relaxometry is an experimental technique that is not only highly sensitive to nanoporous environments, but is also portable, non-destructive, and adapts to a range of sample geometries, making it well-suited to high-throughput process streams and in situ analysis.[13–15] By measuring the transverse relaxation rates of nuclei within a material, one may infer the microscopic pore environment, discriminate between bulk phases, and track dynamic processes in a system such as molecular relaxation, diffusion, and chemical exchange. Probing these dynamic properties of solvent nuclei within an imbibed molecule can therefore elucidate

[*] Dr. S. N. Fricke, M. Salgado, J. Wang, Dr. K. Engler, Dr. Y. Wang
Department of Chemical and Biomolecular Engineering
University of California, Berkeley
Berkeley, CA 94720, USA
E-mail: snfricke@berkeley.edu

Dr. T. Menezes, Dr. K. M. Costa Santos
Department of Process Engineering
Tiradentes University
Aracaju, SE 49010-390, Brazil

Dr. N. B. Gallagher
Chemometrics
Eigenvector Research, Inc.
Manson, WA 98831, USA

Dr. A.-Y. Song, Dr. J. A. Reimer
Department of Chemical and Biomolecular Engineering
University of California, Berkeley
Berkeley, CA 94720, USA
and
Materials Sciences Division
Lawrence Berkeley National Laboratory
Berkeley, CA 94720, USA

Dr. H. Mao
Department of Materials Science and Engineering
Stanford University
Stanford, CA 94305, USA

the geometry of the molecular environment in which the solvent is confined. The transverse relaxation rate, R_2, is inversely related to the T_2 parameter, and in the fast diffusion limit, relates to surface area as:

$$\frac{1}{T_2} = \frac{1}{T_{2b}} + \rho\frac{S}{V} + \frac{1}{12}D_0\gamma^2G^2{t_e}^2 \quad (1)$$

where the first term, $\frac{1}{T_{2b}}$, expresses the bulk relaxation rate.[13,16–18] The second term describes surface relaxation, where ρ indicates surface relaxivity and $\frac{S}{V}$ refers to the pore surface area to volume ratio. The third term accounts for coherence losses caused by inhomogeneities in the local magnetic field, where D_0 is the bulk self-diffusion coefficient, γ is the gyromagnetic ratio of the detected nucleus, G is a magnetic field gradient arising from DC field inhomogeneities or the local pore environment, and t_e is the pulse sequence echo time. There may be multiple pore environments, each with unique surface relaxation, and therefore multiple relaxation rates may occur. The observation of broad distributions of transverse relaxation rates can hinder precise analysis of nanopore geometry directly from T_2 measurement.

Nonetheless, efficient methods to predict pore surface area are necessary to translate NMR relaxometry measurements to high-throughput porosity screenings. Moreover, it is clear from Eq. (1) that there exists a linear relationship between R_2 and the pore surface area to volume ratio, $\frac{S}{V}$, and that developing an empirically based relationship between the two measurements may be possible. To this end, machine learning has emerged as a powerful tool for classification and prediction,[19] and its use is explored here. Machine learning is a widely implemented subfield of artificial intelligence (AI), broadly used for improving algorithms for the distinct purposes of classification and prediction.[20] In the years since its advent in the mid-20th century, the field of machine learning has differentiated from AI by moving toward an approach centered on a probabilistic, statistical view of modeling, and away from algorithms constructed with symbolic logic,[21] thereby maintaining a connection to validation that is essential for practical use. The key elements in a machine learning approach to modeling are, first, pattern recognition to shape a model (versus population inferences to posit a model a priori, as in a purely statistical approach), and second, optimization, often through the use of a loss function.[22] Multilinear algorithms frequently use low-dimensional representations[23] of data predictor and response variables to perform regressions, thereby enabling these models to work seamlessly with tensor representations of high-dimensional and complex data that can be otherwise prohibitively challenging to analyze.[24,25]

Results and Discussion

Clustering of high and low surface area materials based on their NMR signals is accomplished herein with principal component analysis (PCA).[26] PCA is an unsupervised orthogonal linear transformation that projects high-dimensional data into a reduced coordinate system where the variance of the data is maximized. For this study, the NMR relaxometry profiles were baseline corrected, normalized using a 1-norm, and then mean-centered, and the data were collected into a matrix $\mathbf{X}$. Following preprocessing, the eigenvalues and eigenvectors of $\mathbf{X}^T\mathbf{X}$ yield the principal components (PCs). The first few PCs with the largest eigenvalues capture the maximum sum of squares in $\mathbf{X}^T\mathbf{X}$ and correspond to the PCA model of the data $\mathbf{X}$. The PCs are also called the principal axes of the data and the sample scores are given by the projection of $\mathbf{X}$ onto the principal axes. Scores show relationships between the relaxometry profiles and can be plotted to elucidate patterns in the data. Dimensionality reduction is accomplished by retaining only the PCs, i.e. dimensions, that explain the majority of the variance and removing all others.[27]

Partial least squares (PLS) can be used to model a correlation between a matrix of responses $\mathbf{X}$ (here, NMR signals) and a vector of reference measurements $\mathbf{y}$ (pore surface area) using the following model:

$$\mathbf{Xb} = \mathbf{y} + \mathbf{e} \quad (2)$$

where the regression vector $\mathbf{b}$ is typically found by minimizing cross-validation error of $\mathbf{e}^T\mathbf{e}$.[28,29] Here, the SIMPLS algorithm was used to identify the model.[30] In PCA, the PCs are found that maximize capture of sum-of-squares in $\mathbf{X}^T\mathbf{X}$. In contrast, PLS is a regression method that finds rotations of the principal axes called latent variables (LVs) that capture maximum covariance between $\mathbf{X}$ and $\mathbf{y}$. The number of LVs in a PLS model is less than or equal to the number of independent variables in $\mathbf{X}$ and correspond to a full rank sub-space that provides an approximation of $\mathbf{X}$ that is most related to $\mathbf{y}$.

In comparison to traditional linear regression, PLS offers a mechanism for dealing with variance due to noise because the regression is performed in the low-dimensional LV space wherein the component number limits the number of regression factors. Further, multi-collinearity—for example, between correlated variables of solvent content and the multi-exponential signal in terms of its ratio of decay rates—causes traditional regression methods to fail, but is handled with ease with PLS.

To demonstrate the ability of the PLS model to provide predictions of pore surface area from NMR signals, the data were split into a calibration set used to identify $\mathbf{b}$ and a test set to assess predictive performance. As described in the Supporting Information Appendix, the majority of the data collected at varying solvent contents was used for calibration, and an additional subset collected at saturation was used for subsequent validation.

Transformation of an NMR signal that decays due to transverse relaxation can yield T_2 distributions, as demonstrated in Figure 1. This has been the common way to infer pore environment through NMR relaxometry historically when a solvent is imbibed within a porous structure, as surface relaxation and pore confinement enhance relaxation and introduce a fast relaxation component.[14,15] However,

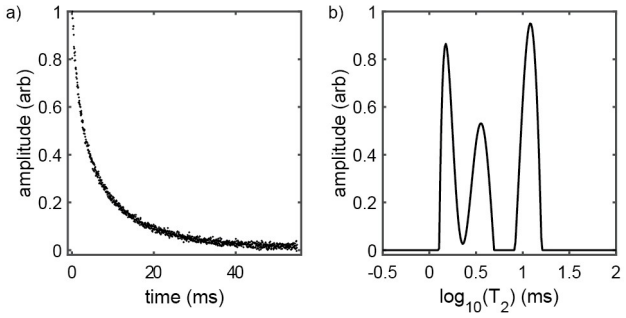

Figure 1. a) Exemplary NMR relaxometry data from a single CPMG experiment in the time domain, shown inverted in b) to a distribution of T_2 via inverse Laplace transform. This experiment was performed on MOF-808(Cr) with 0.9 mL/g of water to provide a signal from inside and outside of the pores, corresponding to short and long T_2 values, respectively. The intermediate T_2 can indicate an additional, large pore structure is present or can be attributed to interfacial water.

this approach rapidly becomes complicated when changes in the macroscopic solvent content or microscopic distribution of solvent affect the ratio and number of unique relaxation components. Moreover, the presence of multiple sizes of pores can introduce multiple R_2, and hence T_2 values, which may be impossible to definitively separate from the effects of surface relaxation from nuclei localized at the pore walls or throat, versus in the pore centers, using an NMR experiment alone.

As solvent is incrementally added to an activated MOF, as shown in Figure 2, the small pores indicated by the faster relaxing component fill first, starting with localization of solvent molecules on the pore walls (i.e., fastest relaxation with the largest R_2 and shortest T_2). This T_2 component lengthens as solvent is added, and when it stops changing and pores are filled, a long T_2 appears, representing bulk water with the smallest R_2. Occasionally, an intermediate T_2 component appears, presumably indicating more freely diffusing solvent molecules in the center of the pore or in exchange between the center of the pore and the bulk water.

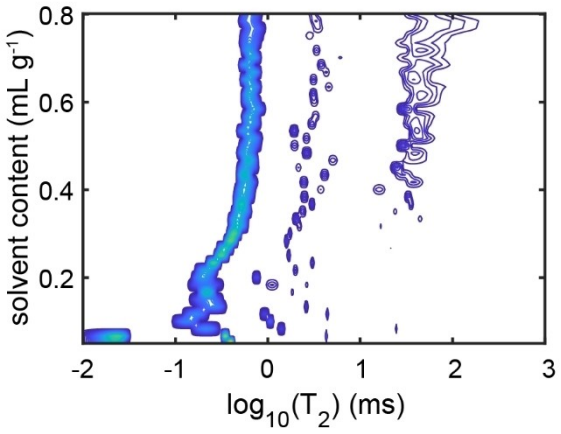

Figure 2. T_2 distributions shown as a function of solvent content with Mg-MOF-meta-74 and water.

However, this can also indicate the presence of a larger pore.

It is therefore advantageous to consider a porosity screening method that bypasses the step of estimating T_2, and is operative at any solvent content. To develop such a screening method, 3-way relaxometry data were collected for 15 materials at varying solvent contents. Figure 3 shows alternative ways that 3-mode data can be organized. Here, the unfolded representation in Figure 3d was used to format all data into a dataset object.[31] Factors that must be considered in choice of data representation are computational efficiency and risk of overfitting.

Following a pre-processing step that included normalizing each transient to unit initial intensity, PCA was performed for bulk clustering of data and detection of outliers. As illustrated in Figure 4, it is immediately evident that surface projection onto a coordinate system of the first three principal components allows separation of low surface area materials (purple) from high surface area materials (yellow), as well as detection of outliers that are amorphous or non-crystalline materials with degraded pore geometry as points that fall outside the shaded 95 % confidence ellipses.

Next, the data were treated with PLS to provide a coarse regression model that is independent of solvent content, as shown in Figure 5. Fifteen materials were tested with an average of twenty solvent contents per material, resulting in over 300 NMR time decays of 1000 points each, and arranged in the unfolded representation of Figure 3d for modeling. Model validation was performed with Venetian blind 10-way cross validation, yielding a linear prediction accuracy of $R^2 = 0.84$ and RMSEC (root mean square error of calibration) of 332.8 m^2/g for all solvent contents.

It is also possible to plot the scores of the data on the first three latent variables to classify data into the color-coded surface area ranges marked by shaded 95 % confidence ellipses. As shown in Figure 6, in a manner similar

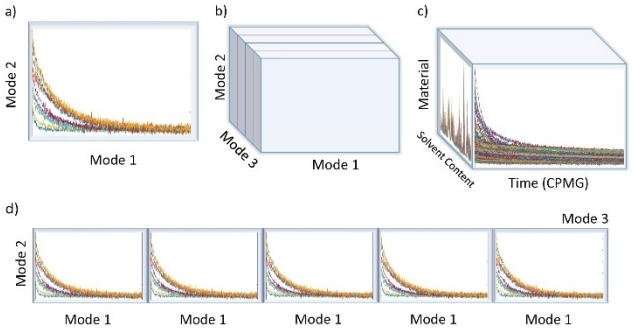

Figure 3. A comparison of data representations suitable for vector- or tensor-based algorithms. In a), a matrix of data is an example of 2-way data that are a function of two variables: here, time (Mode 1) and material (Mode 2). This data representation is suited for vector- or matrix-based algorithms. If a third variable is added, as indicated by Mode 3 in b), the data can be stacked into a 3-way array. A relevant example in c) shows solvent content being introduced as the Mode 3 variable; this form of data is suited for tensor-based algorithms. If the 3-way array of data is "unfolded," or linearly concatenated into an extended 2-way array, it can be treated with vector-based algorithms.

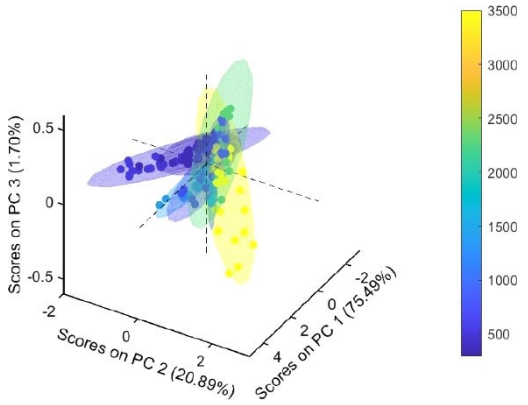

Figure 4. A screening step using 6-component PCA on NMR relaxometry data from different materials at varying solvent content to separate materials based on surface area by plotting their scores on the first three principal components (PC). Surface areas (in m^2/g) are color coded on a gradient from low (purple) to high (yellow). It is also possible to separate amorphous or non-crystalline materials with degraded pore geometry by identifying any point that falls outside the shaded 95% confidence ellipses.

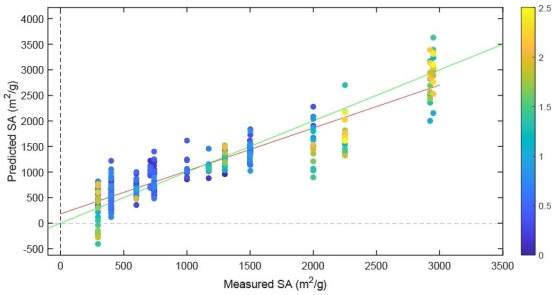

Figure 5. Surface area prediction using the PLS model on NMR relaxometry data from different materials at varying solvent. The 1:1 diagonal line is indicated in solid green, and the fit line is indicated in red. Total RMSEC is 332.8 m^2/g, corresponding to a linear fit R^2 value of 0.84. Cross validation was performed using Venetian blinds with 10 splits and a blind thickness of 1. The horizontal axis indicates the BET surface area whereas the vertical axis indicates the predicted surface area from an NMR relaxometry measurement at any solvent content. Solvent content (in mL/g) is color coded on a gradient from low (purple) to high (yellow).

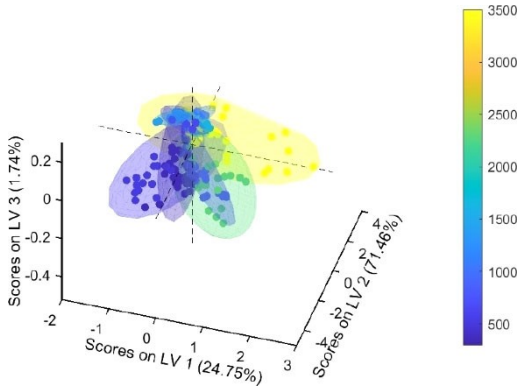

Figure 6. Scores on the first three latent variables (LV) from the 6-component PLS model of NMR relaxometry data from different materials at varying solvent content. Cross validation was performed using Venetian blinds with 10 splits and a blind thickness of 1. Surface areas (in m^2/g) are color coded on a gradient from low (purple) to high (yellow).

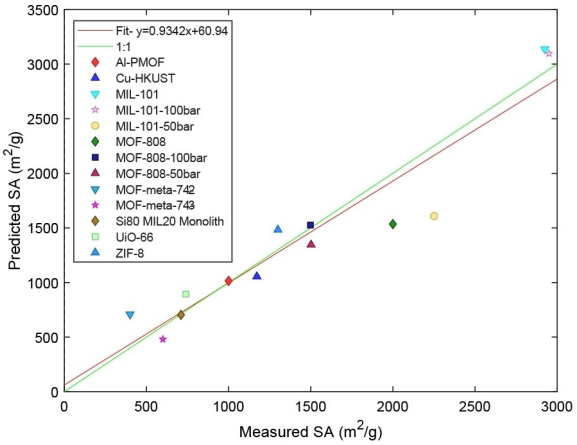

Figure 7. Surface area prediction of test samples using the PLS model on NMR relaxometry data at the most saturated solvent content of 2.5 mL water per gram material. The 1:1 diagonal line is indicated in solid green, and the fit line is indicated in red.

to the PCA approach, examination of the first three latent variables also offers a convenient way to perform rapid classification of materials based on their differing surface area.

By splitting the data into a calibration set and a separate validation set, it is possible to test the predictive capability of the PLS model. Here, a separate set of solvent-saturated samples were measured with NMR to test the PLS model on new data; the results are reported in Figure 7. The root mean square error of prediction, or RMSEP, is 263.5 m^2/g. Because the signal-to-noise increases with solvent content, this suggests that NMR testing of solvent-saturated samples is the best choice of solvent content for future material analysis in this way. Further PLS model details are summarized in Section III of the Supporting Information Appendix.

It would be beneficial to calibrate similar PCA and PLS models based on other solvents to provide an alternative for materials known to lack stability in water. Ideally, the choice of solvent could be matched to the synthesis so that drying in the final step may be bypassed for this screening.

In summary, this screening method may be carried out by following a protocol that involves the following steps. First, a solvent (here, water) is added to a prepared material in a vessel suitable for NMR measurement at any concentration to yield a mixture with the consistency of a slurry. Next, an echo train NMR experiment is performed as described in Section II of the Supporting Information Appendix. When the material is saturated with proton-rich solvent, signal is abundant and sufficient signal-to-noise is typically acquired within 30–60 seconds of scans. Immediately after it is recorded, the time decay of the echo train is

input to the calibrated PCA and PLS models, whose outputs are generated within a few seconds.

Conclusion

The purpose of the PCA classification and PLS regression models presented here demonstrate the utility of a machine learning approach for rapid screening of materials in a high-pass sense. We propose this method as an easily calibrated, benchtop tool that can be operated directly in a synthetic chemistry lab with minimal interruption to workflow. This approach offers a high-throughput, non-destructive way to assess porosity in ~1 minute, resulting in a pore surface area estimate ~1440 times faster than a gas adsorption isotherm measurement which requires ~1 day to perform. The technique proposed here is sensitive to pore sizes in the range of approximately 0.5–100 nm and can be used to characterize the pore structure of a wide range of materials. The materials that pass this screening technique by clustering with high surface area materials would be identified as potential candidates to undergo more accurate and time-intensive porosity testing via BET analysis of gas adsorption isotherms. Coupled together in this way, the throughput and efficiency of synthetic labs could be greatly enhanced.

Supporting Information

The authors have cited additional references within the Supporting Information.[31–46]

Acknowledgements

Support from The *USorb-DAC* Project, funded by a grant from The Grantham Foundation for the Protection of the Environment to RMI's climate tech accelerator program, Third Derivative, is gratefully acknowledged. Partial support was also provided by the Department of Energy Office of Science, Office of Basic Energy Sciences, under Award DESC0019992. The authors wish to thank Dr. Joseph Chen for advice and inspiration, Dr. Velencia Witherspoon for insightful conversations, and Dr. Nicholas Settineri and the UC Berkeley CheXray crystallographic facility for their help in the collection of powder X-ray diffraction data.

Conflict of Interest

NG is an employee of the company Eigenvector Research, Inc., whose software was used in this study.

Data Availability Statement

The data that support the findings of this study are available from the corresponding author upon reasonable request.

Keywords: metal-organic frameworks · porous materials · machine learning · NMR relaxometry

[1] J. R. Long, O. M. Yaghi, *Chem. Soc. Rev.* **2009**, *38*, 1213.
[2] E. Braun, J. J. Chen, S. K. Schnell, L. Lin, J. A. Reimer, B. Smit, *Angew. Chem. Int. Ed.* **2015**, *54*, 14349–14352.
[3] P. H. Emmett, S. Brunauer, *J. Am. Chem. Soc.* **1937**, *59*, 1553–1564.
[4] S. Brunauer, P. H. Emmett, E. Teller, *J. Am. Chem. Soc.* **1938**, *60*, 309–319.
[5] E. P. Barrett, L. G. Joyner, P. P. Halenda, *J. Am. Chem. Soc.* **1951**, *73*, 373–380.
[6] B. B. Mandelbrot, *Phys. Scr.* **1985**, *32*, 257–260.
[7] B. Mandelbrot, *Science (1979)* **1967**, *156*, 636–638.
[8] P. G. Toledo, R. A. Novy, H. T. Davis, L. E. Scriven, *Soil Sci. Soc. Am. J.* **1990**, *54*, 673–679.
[9] H. Jiang, B. Guo, M. L. Brusseau, *Adv. Water Resour.* **2020**, *146*, 103789.
[10] A. Laaksonen, J. Malila, A. Nenes, H.-M. Hung, J.-P. Chen, *Sci. Rep.* **2016**, *6*, 25504.
[11] J. W. M. Osterrieth, J. Rampersad, D. Madden, N. Rampal, L. Skoric, B. Connolly, M. D. Allendorf, V. Stavila, J. L. Snider, R. Ameloot, J. Marreiros, C. Ania, D. Azevedo, E. Vilarrasa-Garcia, B. F. Santos, X. Bu, Z. Chang, H. Bunzen, N. R. Champness, S. L. Griffin, B. Chen, R. Lin, B. Coasne, S. Cohen, J. C. Moreton, Y. J. Colón, L. Chen, R. Clowes, F. Coudert, Y. Cui, B. Hou, D. M. D'Alessandro, P. W. Doheny, M. Dincă, C. Sun, C. Doonan, M. T. Huxley, J. D. Evans, P. Falcaro, R. Ricco, O. Farha, K. B. Idrees, T. Islamoglu, P. Feng, H. Yang, R. S. Forgan, D. Bara, S. Furukawa, E. Sanchez, J. Gascon, S. Telalović, S. K. Ghosh, S. Mukherjee, M. R. Hill, M. M. Sadiq, P. Horcajada, P. Salcedo-Abraira, K. Kaneko, R. Kukobat, J. Kenvin, S. Keskin, S. Kitagawa, K. Otake, R. P. Lively, S. J. A. DeWitt, P. Llewellyn, B. V. Lotsch, S. T. Emmerling, A. M. Pütz, C. Martí-Gastaldo, N. M. Padial, J. García-Martínez, N. Linares, D. Maspoch, J. A. Suárez del Pino, P. Moghadam, R. Oktavian, R. E. Morris, P. S. Wheatley, J. Navarro, C. Petit, D. Danaci, M. J. Rosseinsky, A. P. Katsoulidis, M. Schröder, X. Han, S. Yang, C. Serre, G. Mouchaham, D. S. Sholl, R. Thyagarajan, D. Siderius, R. Q. Snurr, R. B. Goncalves, S. Telfer, S. J. Lee, V. P. Ting, J. L. Rowlandson, T. Uemura, T. Iiyuka, M. A. van der Veen, D. Rega, V. Van Speybroeck, S. M. J. Rogge, A. Lamaire, K. S. Walton, L. W. Bingel, S. Wuttke, J. Andreo, O. Yaghi, B. Zhang, C. T. Yavuz, T. S. Nguyen, F. Zamora, C. Montoro, H. Zhou, A. Kirchon, D. Fairen-Jimenez, *Adv. Mater.* **2022**, *34*, 2201502.
[12] A. De, M. Maliuta, I. Senkovska, S. Kaskel, *Langmuir* **2022**, *38*, 14073–14083.
[13] B. Blümich, J. Perlo, F. Casanova, *Prog. Nucl. Magn. Reson. Spectrosc.* **2008**, *52*, 197–269.
[14] J. J. Chen, X. Kong, K. Sumida, M. A. Manumpil, J. R. Long, J. A. Reimer, *Angew. Chem. Int. Ed.* **2013**, *52*, 12043–12046.
[15] J. J. Chen, J. A. Mason, E. D. Bloch, D. Gygi, J. R. Long, J. A. Reimer, *Microporous Mesoporous Mater.* **2015**, *205*, 65–69.
[16] R. Kimmich, *NMR Tomography, Diffusometry, Relaxometry*, Springer Berlin Heidelberg, Berlin, Heidelberg, **1997**.
[17] P. T. Callaghan, *Translational Dynamics and Magnetic Resonance*, Oxford University Press, **2011**.
[18] B. Blümich, *NMR Imaging of Materials*, Clarendon Press, **2003**.
[19] E. Alpaydin, *Introduction to Machine Learning*, MIT, **2020**.
[20] S. Russell, P. Norvig, *Artificial Intelligence: A Modern Approach*, Prentice Hall, **2003**.
[21] P. Langley, *Mach. Learn.* **2011**, *82*, 275–279.
[22] D. Bzdok, N. Altman, M. Krzywinski, *Nat. Methods* **2018**, *15*, 233–234.

[23] S. T. Roweis, L. K. Saul, *Science (1979)* **2000**, *290*, 2323–2326.
[24] E. Lopez-Fornieles, G. Brunel, F. Rancon, B. Gaci, M. Metz, N. Devaux, J. Taylor, B. Tisseyre, J.-M. Roger, *Remote Sens. (Basel)* **2022**, *14*, 216.
[25] A. Eliseyev, V. Auboiroux, T. Costecalde, L. Langar, G. Charvet, C. Mestais, T. Aksenova, A.-L. Benabid, *Sci. Rep.* **2017**, *7*, 16281.
[26] R. Bro, A. K. Smilde, *Anal. Methods* **2014**, *6*, 2812–2831.
[27] Y. Kusaka, T. Hasegawa, H. Kaji, *J. Phys. Chem. A* **2019**, *123*, 10333–10338.
[28] H. Martens, T. Næs, *Multivariate Calibration*, John Wiley & Sons, Chichester, **1989**.
[29] S. Wold, M. Sjöström, L. Eriksson, *Chemom. Intell. Lab. Syst.* **2001**, *58*, 109–130.
[30] S. de Jong, *Chemom. Intell. Lab. Syst.* **1993**, *18*, 251–263.
[31] Eigenvector Research Inc., **2023**.
[32] G. Férey, C. Mellot-Draznieks, C. Serre, F. Millange, J. Dutour, S. Surblé, I. Margiolaki, *Science (1979)* **2005**, *309*, 2040–2042.
[33] J. E. Efome, D. Rana, T. Matsuura, C. Q. Lan, *Sci. Total Environ.* **2019**, *674*, 355–362.
[34] H. Furukawa, F. Gándara, Y.-B. Zhang, J. Jiang, W. L. Queen, M. R. Hudson, O. M. Yaghi, *J. Am. Chem. Soc.* **2014**, *136*, 4369–4381.
[35] E. S. Grape, J. G. Flores, T. Hidalgo, E. Martínez-Ahumada, A. Gutiérrez-Alejandre, A. Hautier, D. R. Williams, M. O'Keeffe, L. Öhrström, T. Willhammar, P. Horcajada, I. A. Ibarra, A. K. Inge, *J. Am. Chem. Soc.* **2020**, *142*, 16795–16804.
[36] B. Blümich, J. Anders, *Magnetic Resonance* **2021**, *2*, 149–160.
[37] J. Perlo, F. Casanova, B. Blümich, *J. Magn. Reson.* **2005**, *176*, 64–70.
[38] G. Eidmann, R. Savelsberg, P. Blümler, B. Blümich, *J. Magn. Reson. Ser. A* **1996**, *122*, 104–109.
[39] H. Y. Carr, E. M. Purcell, *Phys. Rev.* **1954**, *94*, 630–638.
[40] S. Meiboom, D. Gill, *Rev. Sci. Instrum.* **1958**, *29*, 688–691.
[41] C. L. Lawson, R. J. Hanson, *Solving Least Squares Problems*, Prentice-Hall, Englewood Cliffs, N. J., **1974**.
[42] R. F. Ling, C. L. Lawson, R. J. Hanson, *J. Am. Stat. Assoc.* **1977**, *72*, 930.
[43] N. P. Domingues, S. M. Moosavi, L. Talirz, K. M. Jablonka, C. P. Ireland, F. M. Ebrahim, B. Smit, *Commun. Chem.* **2022**, *5*, 170.
[44] M. T. Kapelewski, S. J. Geier, M. R. Hudson, D. Stück, J. A. Mason, J. N. Nelson, D. J. Xiao, Z. Hulvey, E. Gilmour, S. A. FitzGerald, M. Head-Gordon, C. M. Brown, J. R. Long, *J. Am. Chem. Soc.* **2014**, *136*, 12119–12129.
[45] D. Feng, W.-C. Chung, Z. Wei, Z.-Y. Gu, H.-L. Jiang, Y.-P. Chen, D. J. Darensbourg, H.-C. Zhou, *J. Am. Chem. Soc.* **2013**, *135*, 17105–17110.
[46] M. Muschi, S. Devautour-Vinot, D. Aureau, N. Heymans, S. Sene, R. Emmerich, A. Ploumistos, A. Geneste, N. Steunou, G. Patriarche, G. De Weireld, C. Serre, *J. Mater. Chem. A* **2021**, *9*, 13135–13142.

Manuscript received: November 2, 2023
Accepted manuscript online: January 30, 2024
Version of record online: February 19, 2024